Volume 9
Number 11
November 2024
Pages 1845–2072

Nanoscale Horizons

The home for rapid reports of exceptional significance in nanoscience and nanotechnology

rsc.li/nanoscale-horizons

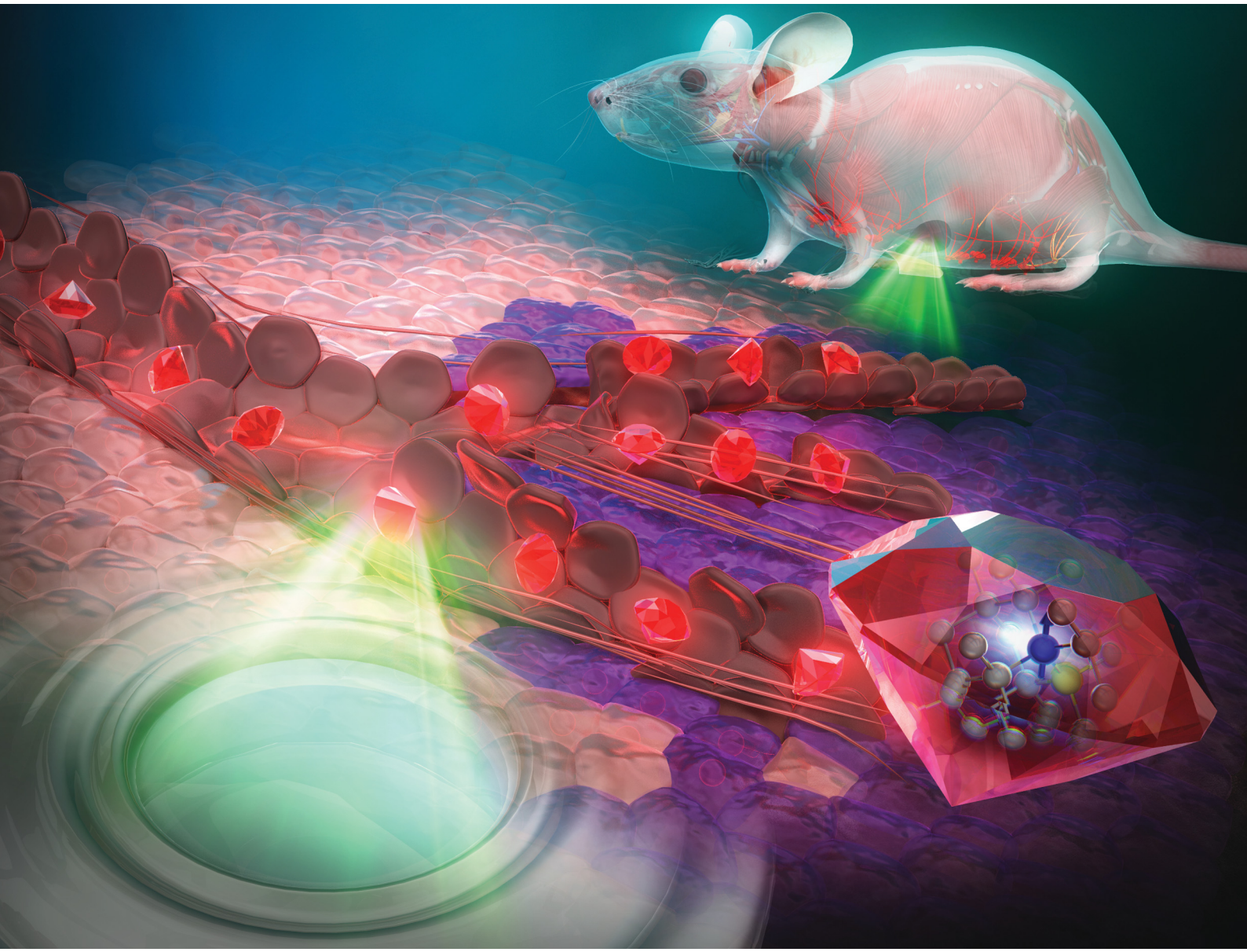

ISSN 2055-6756

ROYAL SOCIETY OF CHEMISTRY

COMMUNICATION
Tatsuhiko Imaoka *et al.*
Intravital microscopic thermometry of rat mammary epithelium by fluorescent nanodiamond

NCNST

Nanoscale Horizons

ROYAL SOCIETY OF CHEMISTRY

COMMUNICATION

View Article Online
View Journal | View Issue

Cite this: *Nanoscale Horiz.*, 2024, **9**, 1938

Received 25th May 2024,
Accepted 29th August 2024

DOI: 10.1039/d4nh00237g

rsc.li/nanoscale-horizons

Intravital microscopic thermometry of rat mammary epithelium by fluorescent nanodiamond†

Takahiro Hamoya,[ab] Kiichi Kaminaga,[ac] Ryuji Igarashi,[acdef] Yukiko Nishimura,[c] Hiromi Yanagihara,[ac] Takamitsu Morioka,[ac] Chihiro Suzuki,[a] Hiroshi Abe,[g] Takeshi Ohshima[g] and Tatsuhiko Imaoka*[ac]

Quantum sensing using the fluorescent nanodiamond (FND) nitrogen-vacancy center enables physical/chemical measurements of the microenvironment, although application of such measurements in living mammals poses significant challenges due to the unknown biodistribution and toxicity of FNDs, the limited penetration of visible light for quantum state manipulation/measurement, and interference from physiological motion. Here, we describe a microenvironmental thermometry technique using FNDs in rat mammary epithelium, an important model for mammary gland biology and breast cancer research. FNDs were injected directly into the mammary gland. Microscopic observation of mammary tissue sections showed that most FNDs remained in the mammary epithelium for at least 8 weeks. Pathological examination indicated no obvious change in tissue morphology, suggesting negligible toxicity. Optical excitation and detection were performed through a skin incision. Periodic movements due to respiration and heartbeat were mitigated by frequency filtering of the signal. Based on these methods, we successfully detected temperature elevation in the mammary epithelium associated with lipopolysaccharide-induced inflammation, demonstrating the sensitivity and relevance of the technique in biological contexts. This study lays the groundwork for expanding the applicability of quantum sensing in biomedical research, providing a tool for real-time monitoring of physiological and pathological processes.

New concepts

We report an application of microscopic thermometry in a living rat using quantum sensing based on the diamond nitrogen-vacancy center (NVC). Although the application of NVC-based quantum sensing (especially those with nanodiamonds) for biomedical use has been anticipated, the application has been limited to small systems such as cultured cells and nematode worms, with no application in living mammals reported to date. This is due to obstacles related to the large difference in both spatial and temporal scales, including the dispersion of injected nanodiamonds in the body, the inability of visible light required for NVC-based measurements to penetrate thick tissue, large physiological movements compared to the size of the microscopic field, and the unknown mid- to long-term toxicity of nanodiamonds. This study overcame each of these barriers by combining quantum sensing with sophisticated laboratory animal techniques, extensive analysis of the localization and toxicity of injected nanodiamonds, and ingenuity in signal processing to mitigate the effect of movements, and ultimately realized the detection of temperature elevation induced by mastitis in the rat. Thus, this study demonstrates the relevance of the technique in biomedical research using a laboratory mammal and lays the groundwork for expanding the applicability of quantum sensing.

Introduction

The importance of body temperature for life is not fully clear.[1] Chemical reactions in organisms require a certain temperature, and therefore, heat is required for proper function.[2] Extreme heat is detrimental, however, and some organs require extensive cooling.[3]

[a] *Institute for Quantum Life Science, National Institutes for Quantum Science and Technology, 4-9-1 Anagawa, Inage-ku, Chiba 263-8555, Japan. E-mail: imaoka.tatsuhiko@qst.go.jp*
[b] *Department of Molecular-Targeting Prevention, Graduate School of Medical Science, Kyoto Prefectural University of Medicine, Kawaramachi-Hirokoji, Kajii-cho, Kamigyo-ku, Kyoto 602-8566, Japan*
[c] *Department of Radiation Effects Research, Institute for Radiological Science, National Institutes for Quantum Science and Technology, 4-9-1 Anagawa, Inage-ku, Chiba 263-8555, Japan*
[d] *School of Life Science and Technology, Tokyo Institute of Technology, 2-12-1 Okayama, Meguro-ku, Tokyo 152-8550, Japan*
[e] *Graduate School of Science and Engineering, Chiba University, 1-33 Yayoi-cho Inage-ku, Chiba 263-8522, Japan*
[f] *Graduate School of Medicine, Tohoku University, 2-1 Seiryo-machi, Aoba-ku, Sendai 980-8575, Japan*
[g] *Quantum Materials and Applications Research Center, Takasaki Institute for Advanced Quantum Science, National Institutes for Quantum Science and Technology, 1233 Watanuki-machi, Takasaki 370-1207, Japan*

† Electronic supplementary information (ESI) available. See DOI: https://doi.org/10.1039/d4nh00237g

The temperature within cells varies among organelles. For example, the nucleus and mitochondria are at higher temperatures, and tend to fluctuate with activity levels, although the role of these temperature fluctuations is underexplored.[4] The mammary gland is a defining organ in mammals, a group of animals that use milk to nourish their offspring. The glandular epithelium is situated within subcutaneous fat tissue, which has thermogenic capacity.[5] The location of the gland on the body surface enables use of thermography to identify pathological conditions such as mastitis (*i.e.*, inflammation of the mammary gland) and breast cancer; therefore, the mammary gland is a compelling subject for research regarding the impact of temperature on biology.

Quantum sensors utilize quantum phenomena to measure physical parameters. The negatively charged nitrogen-vacancy center (NVC) in diamond is a lattice defect consisting of a nitrogen atom adjacent to a vacancy; the NVC provides a unique system in which one can manipulate and measure the spin state of an electron pair at ambient temperature.[6] The electron pair of a diamond NVC has ground-($^3A_2$) and excited-state (^3E) triplets with two intermediate-state singlets ($^1A_1$ and ^1E).[7] The energy of the $m_s = \pm1$ state of $^3A_2$ is higher than that of the corresponding $m_s = 0$ state; this allows transition from $m_s = 0$ to $m_s = \pm1$ through application of microwaves at $\sim$2870 MHz.[7] Upon excitation by green light (520–540 nm), the $m_s = 0$ state of ^3E relaxes directly to the $m_s = 0$ state of $^3A_2$, resulting emission of red fluorescence (650–750 nm).[7] By contrast, the $m_s = \pm1$ state of ^3E relaxes either directly to $^3A_2$ (with red fluorescence) or through an intermediate dark state towards $m_s = 0$ of $^3A_2$.[7] These properties allow for $m_s = 0$ polarization of NVCs through continuous irradiation with green light.[7] Thus, the spin state of the NVCs can be manipulated by a combination of microwaves and green light, and the state can be monitored optically by magnetic resonance (ODMR) measurement of red fluorescence. In this method, the NVC is $m_s = 0$ hyperpolarized, followed by exposure to microwaves of a certain frequency. The spin state is read out based on the emitted red fluorescence. The diamond NVC can be used to measure physical quantities such as local temperature and electric/magnetic fields, because the energy gaps among the $m_s = \pm1$ and 0 states are sensitive to these parameters, and also to measure pH, free radicals, and microscopic movements.[8–13]

Fluorescent nanodiamonds (FNDs) are expected to revolutionize measurement in biology and medicine through quantum sensing.[10] Temperature measurements with FNDs have been applied to microscopic biological systems such as nematode worms and cultured neuronal networks to explore the physiological roles played by local temperature.[14–16] Possible barriers to the biomedical application of a nanomaterial include potential toxicity and the presence of biological defense mechanisms that hinder its retention within the body.[17] Thus, researchers have developed ways of manipulating the size, shape, and surface characteristics of various nanomaterials to reduce toxicity and circumvent defense mechanisms, turning them into smart systems for delivery of therapeutic and imaging agents.[17] Another barrier is the difficulty in manipulating and measuring FNDs using devices outside the body; therefore, the relatively external location of the mammary gland makes it an ideal target for optical measurements using diamond NVC-based quantum sensors (visible light cannot penetrate deep into the body). In the present study, we developed a method for delivering FNDs to the mammary epithelium of rats, a laboratory animal model of mastitis and breast cancer. We then evaluated their retention, localization, and toxicity. We also developed a method for using the delivered FNDs to measure the local temperature of the mammary gland.

Experimental

Animal experiments

All animal experiments were approved by the Institutional Animal Care and Use Committee of the National Institutes for Quantum Science and Technology (approval number 18-1029) and were conducted in accordance with institutional guidelines. Female Jcl:SD rats (5 weeks old) were purchased from CLEA Japan (Tokyo, Japan), housed in autoclaved cages, and maintained in a room with controlled temperature (23 $\pm$ 1 °C) and humidity (50 $\pm$ 5%) under a regular 12-h light/dark cycle. They were given a standard laboratory animal diet (CE-2, CLEA Japan) and sterilized chlorinated/acidified water *ad libitum*. At 7 weeks of age, the abdominal hair was shaved under isoflurane anesthesia ($\sim$4% in air) to expose the 4th and 5th nipples. FNDs were produced essentially as described,[12] where nanodiamond powder (median diameter, 200 nm; Micron + MDA 0–0.25 μm, Element Six, London, UK) was electron-irradiated (2 MeV, 1.0×10^{18} electrons cm^{-2}) at room temperature followed by thermal annealing at 800 °C for 2 h under vacuum to create NVCs, oxidized subsequently to remove surface graphite, heated consecutively in H_2SO_4/HNO_3, 0.1 M NaOH, and 0.1 M HCl, and washed with ultrapure water. The average number of NVCs in a FND particle was estimated to be $\sim 1.3 \times 10^3$ (ESI†). FNDs (50 μL) of 1 mg mL^{-1} in Dulbecco's calcium/magnesium-free phosphate-buffered saline containing 0.3% indigo carmine (for visualization of possible leakage) was injected in the nipple using a 34-gauge microinjection needle (Unisys Co., Tokyo, Japan). Animals were excluded from the experiment and euthanized if leakage occurred. Three rats injected with the same type of FNDs were kept in a disposable cage (Shinano Seisakusho, Tokyo, Japan; to avoid cross-contamination and for the safety of workers) for 1, 3, 6, and 8 weeks and 1 year, and then euthanized by exsanguination under isoflurane anesthesia prior to removal of mammary tissue. Rats were nonrandomly allocated to the experimental groups due to the small sample size. Technical staff involved in animal care, tissue collection, and histological sample preparation were blinded to the treatment group. To measure the intraductal temperature, rats were anesthetized by intraperitoneal injection of a mixture of 0.375 mg kg^{-1} bodyweight medetomidine, 2.0 mg kg^{-1} midazolam, and 2.5 mg kg^{-1} butorphanol in 5 mL kg^{-1} of saline. A suspension of FNDs with or without *Escherichia coli* O55:B5 lipopolysaccharide (LPS; 200 ng μL^{-1}; Sigma-Aldrich, St. Louis, MO, USA) was injected in the nipple as described above. After housing,

the abdominal skin was shaved, a ~1-cm incision was created adjacent to the nipple using a clean pair of iris scissors, and a round coverslip (18 mm in diameter, 0.13–0.17 mm thick; #12-545-100, Thermo Fisher, Waltham, MA, USA) was embedded in the incision. For a rat, a round coverslip was attached to the skin without creating an incision. To prevent anesthesia-induced hypothermia during the ODMR measurement, rats were placed on a custom-made heating stage (940 mm × 1400 mm) set at 37 °C and incorporating a slit of 940 mm × 300 mm (Blast Co., Kawasaki, Japan) designed to keep the abdominal surface from direct heating and allow exposure to the objective lens. After the measurements, the rats were euthanized by exsanguination without recovering from anesthesia.

Whole-mount mammary tissue

Mammary tissues were stretched across glass slides, fixed in 10% phosphate-buffered formalin (Fujifilm Wako Chemicals, Osaka, Japan) for 1–3 days, and stored at 4 °C in 70% ethanol. They were then defatted in acetone for 3 days, cleared in *d*-limonene (Falma Inc., Tokyo, Japan) for 2 days, and stored in mineral oil in heat-sealed plastic bags. Bright-field and fluorescence images were taken using an all-in-one fluorescence microscope BZ-X810 (Keyence, Osaka, Japan).

Staining and analysis of tissue sections

Formalin-fixed paraffin-embedded tissues were prepared from a portion of the whole-mount mammary tissue and sectioned at ~4 μm. Sections were stained with HE (Muto Pure Chemicals, Tokyo, Japan) or 4′,6-diamidino-2-phenylindole (DAPI; Vector Laboratories, Newark, CA, USA) and mounted under coverslips. Stained sections were scanned with a NanoZoomer Digital Pathology system (Hamamatsu Photonics, Hamamatsu, Japan). Immunofluorescence staining was performed essentially as described,[18] except that the antigens were reactivated by autoclaving in 0.01 M citrate sodium buffer (pH 6.0) at 121 °C for 10 min and that sections were incubated with rabbit polyclonal anti-nuclear factor κB (NF-κB) antibody (1 : 100; ARG51518, Arigo Laboratories, Hsinchu, Taiwan) at 4 °C overnight and then with secondary antibody (1 : 500; goat anti-rabbit immunoglobulin conjugated with Alexa Fluor 488; Abcam, Cambridge, UK) at room temperature for 1 h. The ImageJ software (National Institutes of Health, Bethesda, MD, USA) was used to measure the areas of fluorescent aggregates.

ODMR measurements

The relevant procedures have been described.[19] Briefly, to record an ODMR frequency spectrum, the microwave output was turned on and off alternately (each frame lasted for 50 ms) while the microwave frequency increased by a step at every two frames. During this process, the sample was continuously irradiated with a green laser (532 nm) for $m_s = 0$ polarization and readout of red fluorescence. The microwave frequency was swept multiple times to accumulate data and enhance reliability. Sweeping between 2820 and 2920 MHz was performed eight times at 1 MHz intervals (*i.e.*, 101 frequency points) to construct an ODMR image of non-HE-stained tissue preparations, and between 2855 and 2885 MHz at 0.075 MHz intervals (*i.e.*, 401 frequency points) in living animals. On occasion, a frequency filter was applied to remove the 0.32–7.0 Hz component of the signal before constructing the ODMR spectrum. The microscopic temperature was evaluated based on the value of the axial zero-field splitting frequency D obtained from the ODMR frequency spectrum of NVCs in FNDs. It is known that D decreases by approximately 75 kHz for every 1 °C increase in temperature.[20] Therefore, we adopted $\Delta D = -75$ kHz K^{-1} as the temperature dependence of D, and used the D value of the FND ensemble measured at 37 °C as the reference frequency. The temperature of the microenvironment was evaluated based on the difference between this reference frequency and the D value of the FND ensemble in the microenvironment. The reference frequency D was obtained by measuring the ODMR frequency spectrum of an FND ensemble in a dish filled with ultrapure water and maintained at a constant temperature of 37 °C. To determine the D value from the ODMR frequency spectrum, a nonlinear model fit was performed using the following function $I(\omega)$, which consists of two Lorentzian functions:

$$I(\omega) = 1 - \frac{c_1}{\pi\gamma\left(1 + \frac{(-D - E + \omega)^2}{\gamma^2}\right)} - \frac{c_2}{\pi\gamma\left(1 + \frac{(-D + E + \omega)^2}{\gamma^2}\right)}$$

where ω is the applied microwave frequency, E corresponds to the Rhombic zero-field splitting, and c_1, c_2, and γ correspond to the signal amplitudes and the half-width at half-maximum of the Lorentzian functions, respectively. The fitting error in the nonlinear model fit was used as the temperature measurement accuracy.

Selective imaging protocol (SIP)

A previously published procedure was followed for the SIP for FNDs based on their sensitivity to microwaves.[21] After excitation with green light, the $m_s = 0$ triplet electrons invariably emit red fluorescence to reach $m_s = 0$ whereas approximately half of the $m_s = \pm 1$ triplet electrons pass through an intermediate (non-fluorescent) singlet state to reach $m_s = 0$, as mentioned above. Thus, green light irradiation for microseconds gathers most of the triplet electrons to $m_s = 0$, while microwave irradiation at the spin resonance frequency (~2870 MHz) increases the proportion of $m_s = \pm 1$ electrons. Due to the longer lifetime of the non-fluorescent singlet state than the excited triplet state, green light irradiation in the presence of microwave for microseconds results in migration of the microwave-induced $m_s = \pm 1$ triplet electrons to the singlet state, and thus, a reduction of fluorescence by 5–10% compared to green light irradiation only.[22] SIP leverages this reduction to distinguish between FNDs and other emitters such as autofluorescence. To construct an image of an HE-stained section using the SIP, video was recorded during microwave irradiation with rectangular intensity modulation synchronized to the camera's frame rate (~50 ms). Images of the microwave-sensitive component of the fluorescence were then generated by subtracting the intensity values of frames with microwave from those without microwave. The sweeping of microwave frequency was performed 1000 times.

Statistical test

Student's *t* test, paired *t* test, and two-way analysis of variance were performed using Microsoft Excel.

Results and discussion

Macroscopic localization and retention of intraductally injected FNDs in non-stained rat mammary gland specimens

Intraductal injection *via* the nipple is a technique used to introduce agents directly into the lumen of the mammary ducts.[23] We used this technique to inject the FND suspensions (1 μg μL^{-1}) into the mammary gland of rats (50 μL per gland). Because surface modification of FNDs contributes markedly to retention, cellular uptake, and aggregation/dispersion,[24,25] we also studied the effects of different surface modifications on the distribution of injected FNDs; these modifications were carboxylation (FND-COOH), hyperbranched polyglycerol (HPG) (FND-HPG), and carboxyl-terminated HPG (FND-HPG-COOH). At 1, 3, 6, and 8 weeks after intraductal injection of FNDs, whole-mount specimens of mammary glands were prepared, and the distribution of FNDs was evaluated by bright-field and fluorescence microscopy (excitation 532 nm/emission 655 nm) (Fig. 1). The results indicated that the intraductally injected

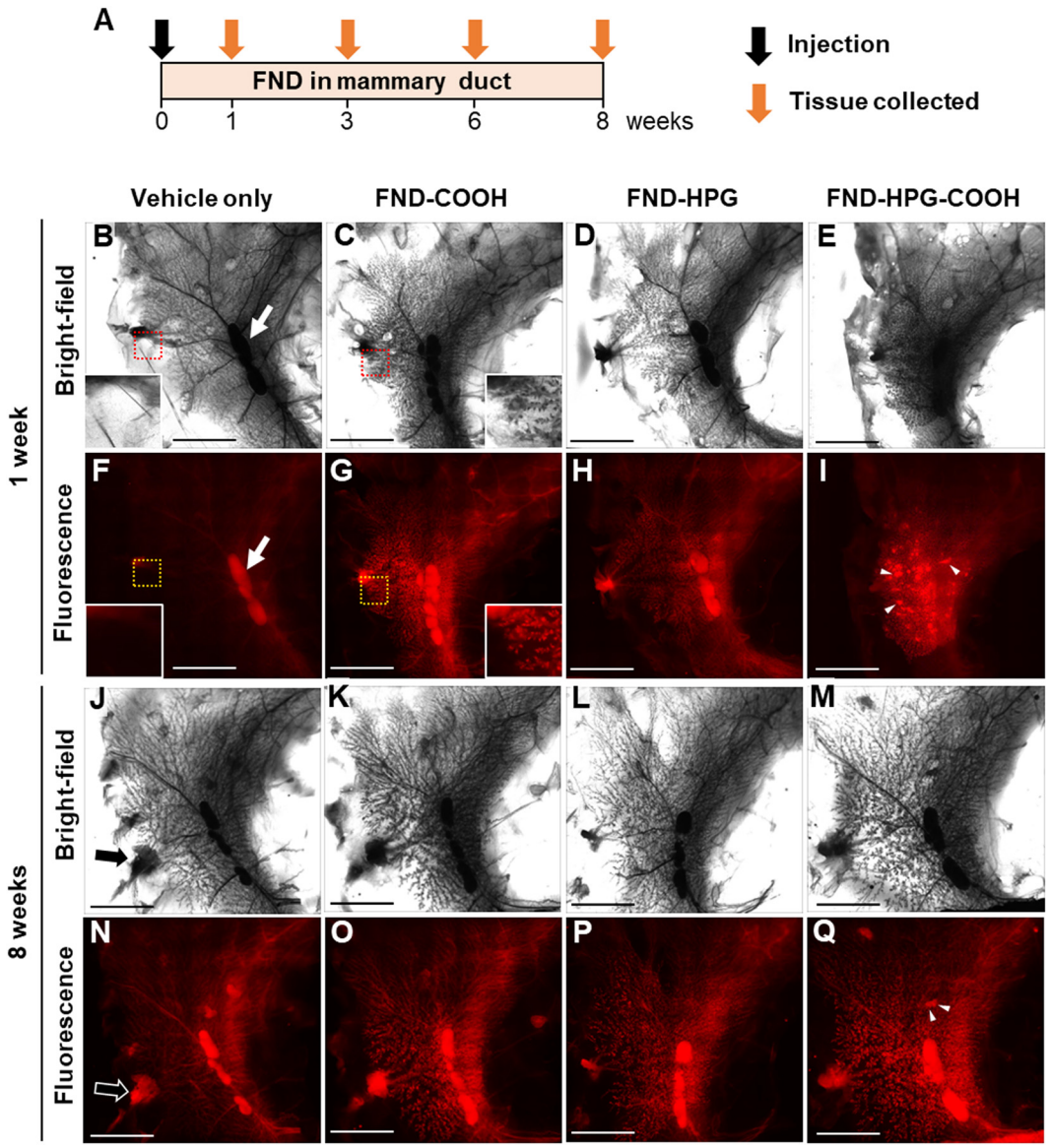

Fig. 1 Detection of FNDs injected in the rat mammary gland. (A) Experimental scheme. FND-X (50 μL, 1 μg μL^{-1}); (X = COOH, HPG, or HPG-COOH) were injected into the abdominal mammary gland of 7-week-old female rats *via* the nipple. Glands were removed after 1, 3, 6, or 8 weeks. (B)–(Q) Bright-field ((B)–(E) and (J)–(M)) and fluorescence (excitation 532 nm, emission, 655 nm; (F)–(I) and (N)–(Q)) images of whole-mount mammary gland specimens at 1 and 8 weeks post-injection. Insets, magnified view of the area bounded by the dashed rectangles. White arrowheads, FND aggregates. The white arrow in panels (B) and (F) shows autofluorescence in the lymph nodes. The black arrow in panels (J) and (N) shows autofluorescence in the nipple. Scale bar, 1 cm. Each panel is a representative for 3 rats.

FNDs were distributed throughout the branching mammary ducts after 1 week (Fig. 1B–I) and remained there at 3, 6, and 8 weeks post-injection (Fig. 1J–Q and Fig. S1, ESI†). At the same concentrations, FND-COOH and FND-HPG-COOH (which are negatively charged) displayed more fluorescence signals than FND-HPG (which is uncharged), possibly due to the high efficiency of cellular uptake and aggregation *via* their surface electrostatic charge.[24] In addition, we found some spot-like depositions of FND-HPG-COOH, which were not associated with the branched network of mammary ducts (Fig. 1I and Q and Fig. S1H and S1P, ESI†). This different localization pattern may be related to the surface modifications. We observed no obvious effect of intraductal injection on the body weight or growth of rats (Fig. S2, ESI†), suggesting that administration of FNDs, at least in this model, is safe.

Microscopic localization and retention of injected FNDs in fluorescence-stained tissue sections

The mammary gland comprises epithelial and stromal components. To further evaluate the localization of injected FNDs

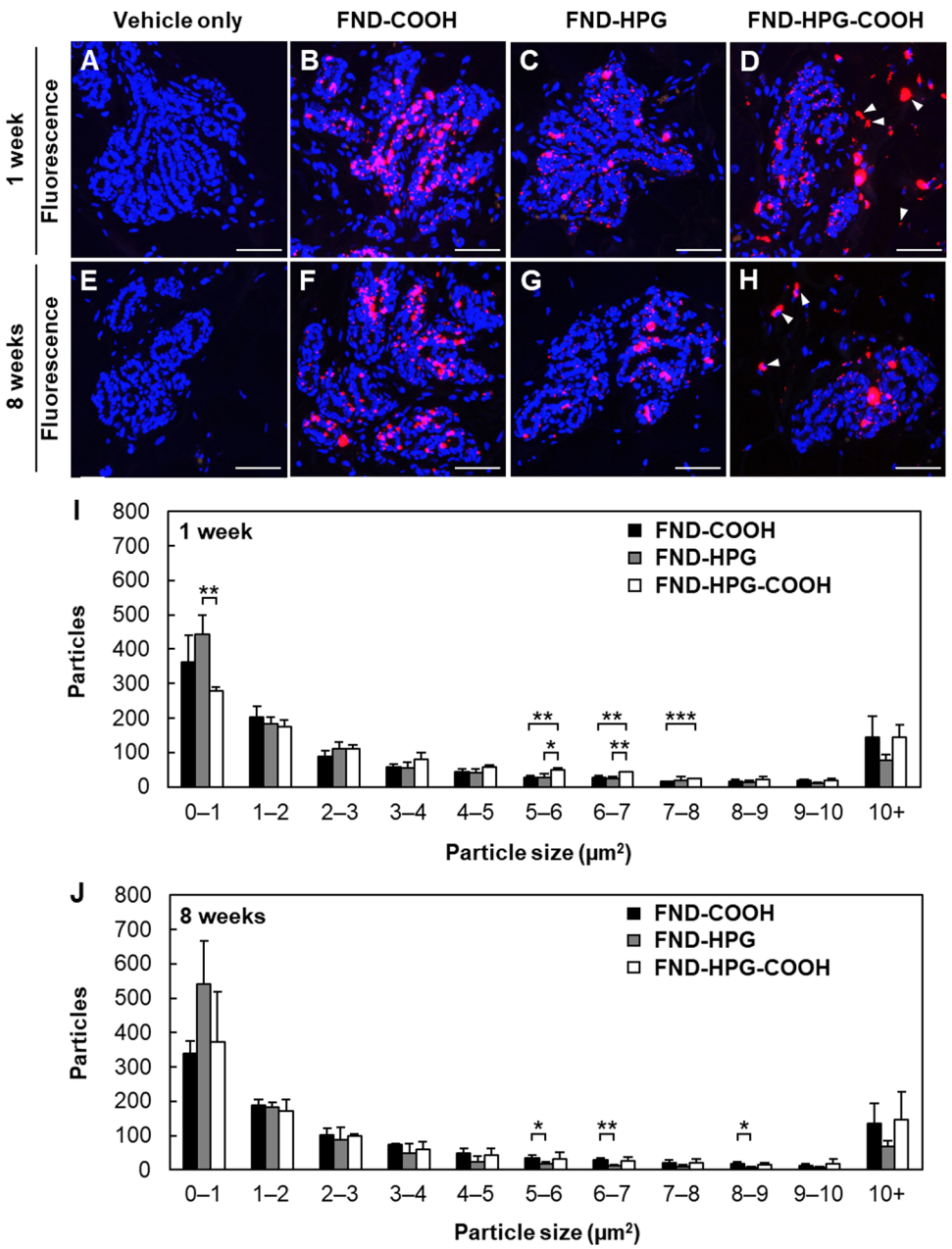

Fig. 2 Localization of FNDs with different surface modifications. (A)–(H) Fluorescence images of DAPI-stained mammary gland tissue sections at 1 and 8 weeks post-injection of vehicle only (A) and (E) or FND-X (X = COOH in (B) and (F), HPG in (C) and (G), and HPG-COOH in (D) and (H)). Red, FND (excitation 532 nm, emission 655 nm). Blue, DAPI. Arrowheads show FNDs in the stromal component. Scale bar, 50 μm. Each panel is a representative for 3 rats. (I) and (J) The size of FND aggregate (n = 1000) in mammary epithelium at 1 (I) and 8 weeks (J) post-injection. Ranges do not include the lower boundary. Data represent the mean and SD (n = 3 rats). * $P < 0.05$, ** $P < 0.01$, *** $P < 0.001$ (Student's t test).

within the mammary gland, we made microscopic preparations of paraffin-embedded sections in which cell nuclei were visualized by DAPI staining (Fig. 2). At 1 week post-injection, FNDs were detected in the mammary epithelium regardless of the type of surface modification (Fig. 2A–D). In addition, FND-HPG-COOH was present in the stromal component of the tissue (Fig. 2D, arrowheads), accounting for the above-mentioned spot-like depositions detected in whole-mount preparations. These FNDs may have been taken up first by ductal epithelial cells *via* endocytosis and then released into the stroma (*i.e.*, transcytosis), or they may have migrated between neighboring ductal epithelial cells (*i.e.*, paracytosis). The transfer mechanism will be a subject for future study. FNDs were observed in the mammary epithelium for at least 8 weeks post-injection (Fig. 2E–H and Fig. S3A–H, ESI†). The size of the FND aggregates in the mammary epithelium was measured to examine the effects of the surface modifications. Among the three types, aggregates of FND-HPG were the smallest, whereas those of FND-COOH and FND-HPG-COOH were larger (Fig. 2I and J and Fig. S3I and J, ESI†).

Tissue toxicity of the injected FNDs, as assessed in conventional tissue section preparations

As mentioned above, injected FNDs remained in the mammary epithelium and formed aggregates. To investigate their potential toxic effects, we conducted histopathological examinations of the

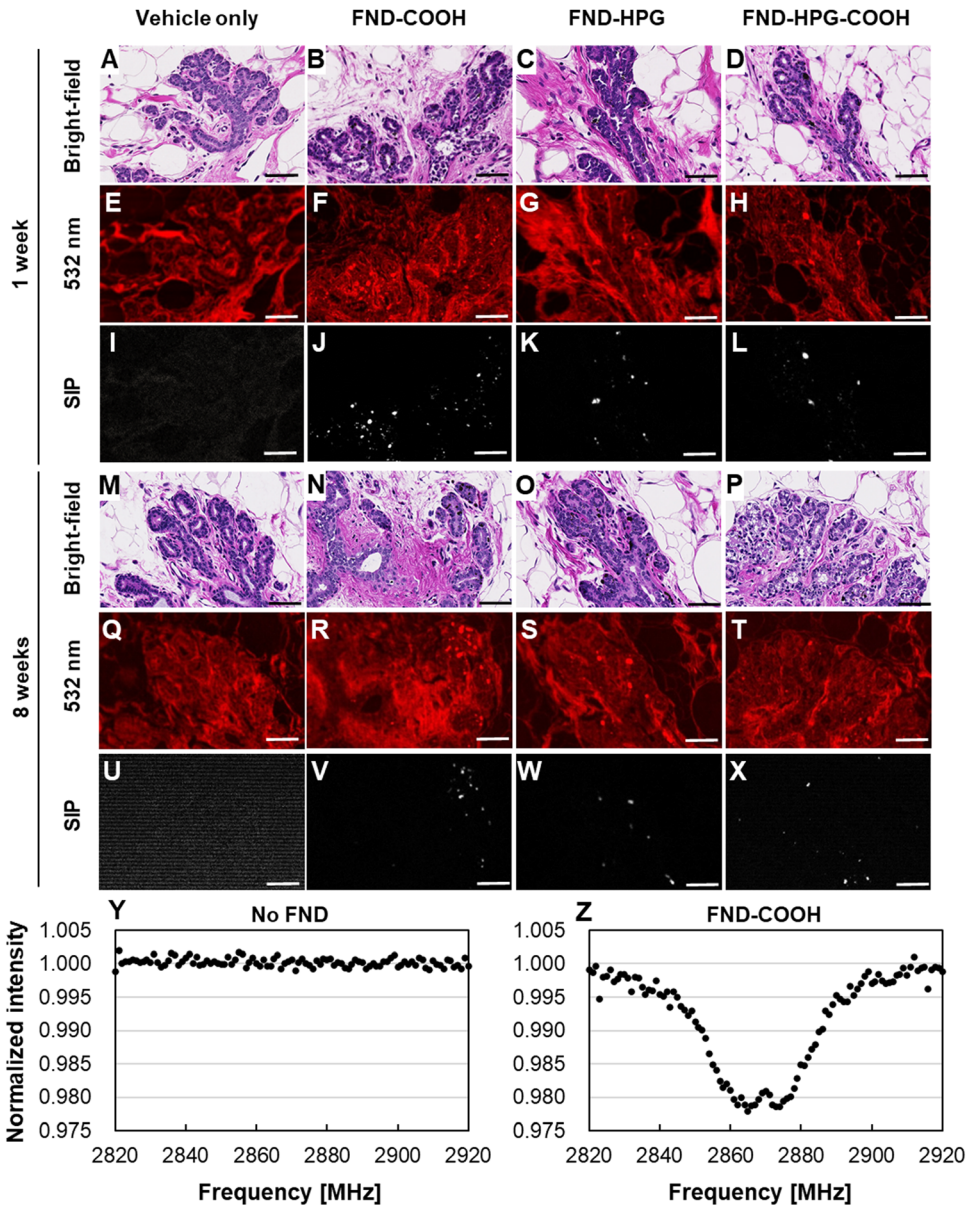

Fig. 3 Histopathology, fluorescence, and selective imaging of FNDs in rat mammary gland tissue sections. (A)–(X) Bright-field ((A)–(D) and (M)–(P)), 532 nm-excited fluorescence ((E)–(H) and (Q)–(T)), and SIP ((I)–(L) and (U)–(X)) images of HE-stained mammary gland tissue sections at 1 and 8 weeks post-injection of vehicle only ((A), (E), (I), (M), (Q), and (U)) or FND-X (X = COOH in (B), (F), (J), (N), (R), and (V); HPG in (C), (G), (K), (O), (S), and (W); and HPG-COOH in (D), (H), (L), (P), (T), and (X)). Scale bar, 50 μm. Each panel is a representative for 3 rats. (Y) and (Z) ODMR spectra obtained from tissue sections from a nontreated rat (Y) and from a rat injected with FND-COOH (Z).

tissue on conventional hematoxylin and eosin (HE)-stained sections. Compared with the fluorescence-stained sections, it was more challenging to locate FNDs in these sections because the strong fluorescence emitted by the HE stains (especially eosin Y) masks the weak fluorescence emitted by FNDs.[26] To circumvent this, we used the SIP to visualize the NVCs.[21] On HE-stained sections, no pathological effects were observed at 1 week or 8 weeks post-injection (Fig. 3A–D and M–P, respectively), regardless of the surface modifications. Although there was marked fluorescence emitted by the HE stain (Fig. 3E–H and Q–T), it was possible to obtain an ODMR spectrum from these specimens (Fig. 3Y and Z). The ODMR signals were strong enough to allow use of the SIP technique, which enabled visualization of the location of FNDs (Fig. 3I–L and U–X). The data suggested no obvious pathological changes had occurred, even in cells in close proximity to FND aggregates.

Intravital microscopic thermometry in the rat mammary gland

Thus far, the data suggest safe and successful delivery of FNDs to the mammary epithelium of rats *via* intraductal injection. Next, we attempted to use FNDs to measure the local temperature of the mammary epithelium (Fig. 4). First, we attempted to obtain ODMR spectra through the intact skin (Fig. S5A and B, ESI†) of a rat and observed spots of strong fluorescence lacking the ODMR spectrum characteristic of FNDs (Fig. 4A and B). Based on their morphology, we considered these spots to be due to autofluorescence by melanin in hair follicles that remained after shaving. Thus, the skin hindered penetration of visible light and acquisition of ODMR spectra for FNDs in the mammary gland. Therefore, we created an incision in the skin of another rat to obtain better ODMR spectra (Fig. S4C and D, ESI†), which resulted in successful observation of fluorescence and improved ODMR spectra for FNDs (Fig. 4C and D). The average measured temperature in an area of the mammary epithelium was 33.72 ± 1.24 °C (mean ± fitting error). This temperature dropped to 27.74 ± 0.51 °C after euthanasia (*i.e.*, death) of the same rat (Fig. 4E and F). Thus, to the best of our knowledge, the present approach is the first to enable measurement of local temperature by NVCs in a living rodent tissue. The lower temperature of the gland than that of the generally assumed one (*i.e.*, ~37 °C) may be due to reduction of body temperature by anesthesia or its relatively external location (note that the heating stage had a 30-mm slit to expose the measured area). Thus, a technique to perform measurements under anesthesia-free conditions, possibly by compact and remote measurement devices, would greatly reduce influences from anesthesia. Using the present method, we were able to detect FNDs in the mammary gland of a rat even after 1 year (Fig. S5, ESI†).

Minimizing the effects of movement due to respiration and heartbeat

During microscopic measurements, we occasionally encountered a periodic "movement" of the fluorescence signal in a

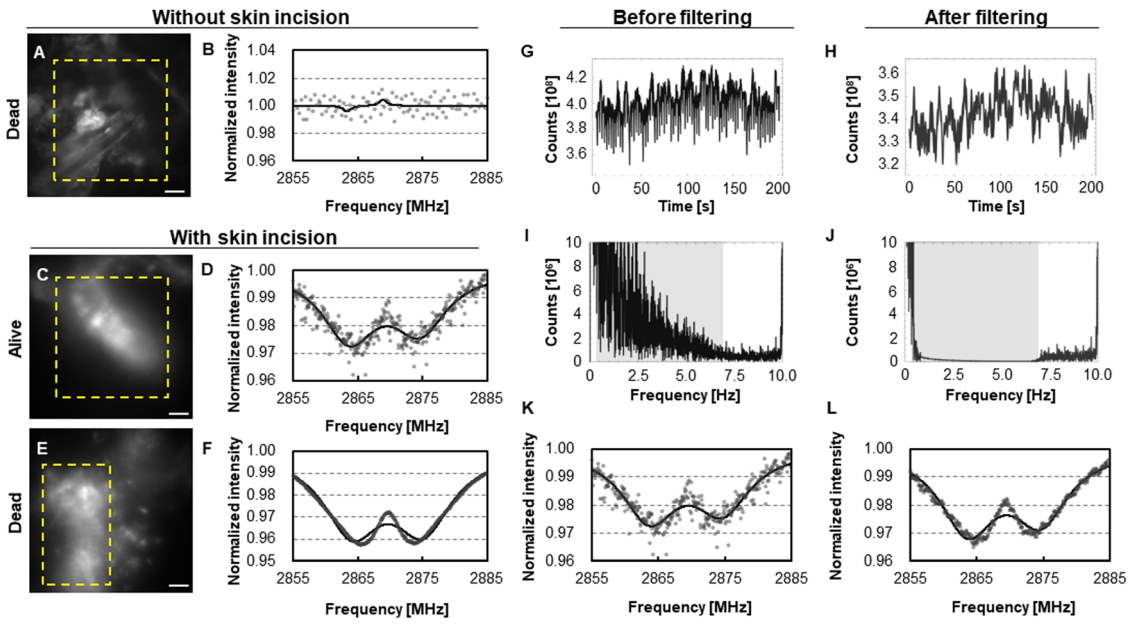

Fig. 4 Thermometry of the mammary epithelium in living rats using FNDs. (A)–(F) Temperature measurements were made after intraductal administration of FND-COOH (200 nm in diameter) into the mammary epithelium. Fluorescence images (20× objective; A, C, and E) and ODMR spectra ((B), (D), and (F)) of FNDs in the dashed rectangles were obtained through the intact skin (A) and (B) or *via* an incision made in the skin (C)–(F) of an anesthetized living rat (C) and (D) or euthanized rats ((A), (B), (E) and (F)). Scale bar ((A), (C), and (E)), 20 μm. (G) and (H) Temporal changes in fluorescence intensity during ODMR spectrometry measurement of FNDs in the rat mammary gland before (G) and after (H) frequency filtering. Frame duration, 50 ms. (I) and (J) Fourier transformation of the signals in panels (G) and (H), respectively. Shading indicates the frequency range to which filtering was applied. (K) and (L) ODMR spectra of FND-COOH (200 nm in diameter) in a living rat, constructed from raw signals ((K), identical to panel (D)) and frequency-filtered signals (L).

living rat (Movie S1, ESI†), which disappeared after euthanasia (Movie S2, ESI†). Based on the periodicity, we surmised that the likely cause was movement due to respiration (~1 Hz) and rhythmic "pulsing" of local blood vessels (~6 Hz).[27] As a result, we encountered profound noise in the ODMR spectrum of FNDs in some rats (compare Fig. 4D and F), resulting in an error in the estimated ODMR spectrum center (0.095 MHz and 0.039 MHz before and after euthanasia, respectively). To improve the accuracy of measurement in such cases, we used data processing to filter signals of a certain frequency, taking advantage of the fact that the signals obtained by the ODMR protocol (Fig. 4G and H for pre- and post-filtering, respectively) comprise frequencies that are different from those caused by respiration and heartbeat (*i.e.*, repetition of spin state initialization/readout, ~10 Hz; repetition of microwave sweeping, ~0.025 Hz; see Fig. 4I and J for pre- and post-filtering, respectively). This improved the shape of the ODMR spectrum and reduced the error when estimating the spectral center frequency from 0.095 MHz (corresponding to 1.24 °C, Fig. 4K) to 0.046 MHz (corresponding to 0.60 °C, Fig. 4L). Thus, the accuracy of temperature measurement using FNDs was improved.

Detection of inflammation-related increases in temperature

Finally, we set out to measure the temperature in the mammary epithelium under pathological conditions. LPS is a bacterial macromolecule composed of lipid and saccharide and stimulates intracellular inflammatory signaling *via* NF-κB.[28] Therefore, we induced an inflammatory response in the mammary gland by intraductal administration of LPS, along with FNDs, and then measured the intramammary temperature. To distinguish the local temperature changes from whole-body temperature elevation, we injected LPS and FNDs into the left mammary gland with only FNDs into the right gland, whereas control rats received only FNDs to both glands (Fig. 5A). Infiltration of inflammatory cells and expression of NF-κB were confirmed in the left mammary gland at 24 h post-administration of LPS (Fig. 5B). When measured by FNDs, LPS treatment resulted in simultaneous temperature elevation (~4 °C) in both mammary glands, possibly as a consequence of whole-body response to LPS (Fig. 5C, asterisk). In addition, the temperature of the mammary gland was higher by ~1 °C in the LPS-injected side than the other side (Fig. 5C, dagger). Thus,

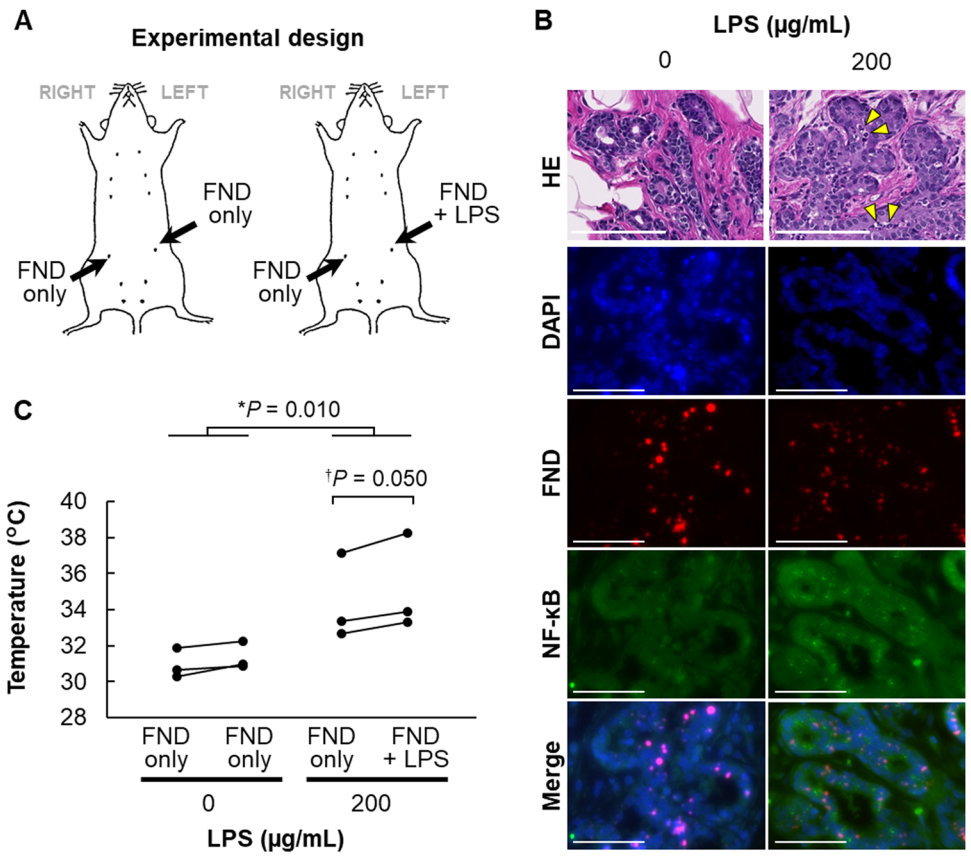

Fig. 5 Intravital microscopic thermometry using intramammary FNDs in an inflammation model. An inflammatory agent, LPS, was injected intraductally into the rat mammary gland, together with FND-COOH (200 nm in diameter). (A) Experimental design (n = 3 rats each). (B) HE sections and immunofluorescence analysis of an inflammation marker, NF-κB, in the mammary gland 24 h after LPS treatment. Yellow arrowheads indicate inflammatory cell infiltration. DAPI (blue) was used to label cell nuclei. FND, fluorescence emitted at a wavelength of 532 nm. NF-κB, immunofluorescence indicating the inflammation marker NF-κB. Merged, merged image. Scale bar, 100 μm. Representative of 3 rats. (C) Measurement of intramammary temperature 24 h after administration of LPS. *Two-way analysis of variance. †Paired t test.

temperature measurement using FNDs can detect an increase in intramammary temperature caused by inflammation.

With respect to errors in intravital temperature measurements with fluorescent nanodiamonds, ± 0.27 °C and ± 0.22 °C have been achieved in nematodes,[14,15] and ± 0.60 °C was achieved in the rat mammary gland in this study. These are sufficient to detect the results of experimental temperature manipulations such as an infrared laser and a mitochondrial deconjugating agent, as well as temperature changes (0.5–1 °C or higher) associated with an extreme pathological condition such as mastitis. However, it is also known that intracellular mechanisms can sense even smaller temperature changes, such as 0.2 °C,[29] and thus it is expected to become even more practical if sensitivity at the ±0.05 °C level can be achieved. One approach to increase sensitivity is a hybrid sensor that takes advantage of the higher sensitivity of NVCs with respect to magnetic measurements than direct temperature measurements.[30] Going forward, it is expected that this method will be applied to temperature measurements in cells and organisms to demonstrate the high sensitivity of this method.

Temperature measurement has been used to screen inflammation and cancer of the breast in clinical and livestock settings.[31,32] The relationship between cancer and temperature has been gradually unraveled by the recent development of thermometric fluorescent probes,[33] but innovative results have yet to be revealed. FND-based thermometry has advantageous properties over previous molecular thermometric probes,[34] including long-term retention and low toxicity of the probe and no requirements for calibration. We have previously reported studies in which breast cancer was induced in rats by administration of carcinogenic chemicals and ionizing radiation.[35–37] Therefore, it is possible to evaluate the relationship between temperature and cancer in this biological model using FNDs.

Conclusions

Here, we show that intraductally administered FNDs are retained for up to 1 year without obvious toxicity. We used ODMR spectrometry to measure the temperature in the microenvironment of the rat mammary gland. Accurate measurement was achieved by canceling the frequencies generated by respiratory and heartbeat movements, leading to successful detection of temperature change related to experimentally induced inflammation. The technique will be potentially useful for monitoring progression of various diseases including cancer. In addition, this experimental model can be applied to quantum measurement of other microenvironmental factors such as pH and radicals.

Author contributions

Takahiro Hamoya (formal analysis: lead; investigation: lead; writing – original draft: lead), Kiichi Kaminaga (investigation: equal; writing – review & editing: equal), Ryuji Igarashi (investigation: equal; methodology: lead; writing – review & editing: lead), Yukiko Nishimura (investigation: equal; writing – review & editing: supporting), Hiromi Yanagihara (investigation: supporting; writing – review & editing: supporting), Takamitsu Morioka (investigation: supporting; writing – review & editing: supporting), Chihiro Suzuki (investigation: supporting; writing – review & editing: supporting), Hiroshi Abe (investigation: supporting; writing – review & editing: supporting), Takeshi Ohshima (investigation: supporting; writing – review & editing: supporting), and Tatsuhiko Imaoka (conceptualization: lead; formal analysis: supporting; project administration: lead; supervision: lead; writing – original draft: lead).

Data availability

The data supporting this article have been included as part of the ESI.†

Conflicts of interest

There are no conflicts to declare.

Acknowledgements

The authors thank Dr Kento Nagata, Ms Masami Ootawara, and Ms Misuzu Fujita for technical support (animal experiments and pathology). This study was supported by MEXT Quantum Leap Flagship Program (MEXT Q-LEAP, grant numbers JPMXS0120330644 and JPMXS0118067395) and by the Cabinet Office of Japan *via* the Public/Private R&D Investment Strategic Expansion Program (PRISM).

References

1 B. D. Knapp and K. C. Huang, *Annu. Rev. Biophys.*, 2022, **51**, 499–526.
2 M. Suzuki, C. Liu, K. Oyama and T. Yamazawa, *J. Biochem.*, 2023, **174**, 217–225.
3 P. S. Yarmolenko, E. J. Moon, C. Landon, A. Manzoor, D. W. Hochman, B. L. Viglianti and M. W. Dewhirst, *Int. J. Hyperthermia*, 2011, **27**, 320–343.
4 M. Suzuki and T. Plakhotnik, *Biophys. Rev.*, 2020, **12**, 593–600.
5 S. Patel, N. Z. R. Sparman, D. Arneson, A. Alvarsson, L. C. Santos, S. J. Duesman, A. Centonze, E. Hathaway, I. S. Ahn, G. Diamante, I. Cely, C. H. Cho, N. K. Talari, A. K. Rajbhandari, L. Goedeke, P. Wang, A. J. Butte, C. Blanpain, K. Chella Krishnan, A. J. Lusis, S. A. Stanley, X. Yang and P. Rajbhandari, *Nature*, 2023, **620**, 192–199.
6 I. Aharonovich, A. D. Greentree and S. Prawer, *Nat. Photonics*, 2012, **5**, 397–405.
7 T. F. Segawa and R. Igarashi, *Prog. Nucl. Magn. Reson. Spectrosc.*, 2023, **134–135**, 20–38.
8 M. Fujiwara and Y. Shikano, *Nanotechnology*, 2021, **32**, 482002.

9 G. Kucsko, P. C. Maurer, N. Y. Yao, M. Kubo, H. J. Noh, P. K. Lo, H. Park and M. D. Lukin, *Nature*, 2013, **500**, 54–58.
10 J. Xu and E. K. Chow, *SLAS Technol.*, 2023, **28**, 214–222.
11 L. P. McGuinness, Y. Yan, A. Stacey, D. A. Simpson, L. T. Hall, D. Maclaurin, S. Prawer, P. Mulvaney, J. Wrachtrup, F. Caruso, R. E. Scholten and L. C. Hollenberg, *Nat. Nanotechnol.*, 2011, **6**, 358–363.
12 T. Fujisaku, R. Tanabe, S. Onoda, R. Kubota, T. F. Segawa, F. T. So, T. Ohshima, I. Hamachi, M. Shirakawa and R. Igarashi, *ACS Nano*, 2019, **13**, 11726–11732.
13 R. Igarashi, T. Sugi, S. Sotoma, T. Genjo, Y. Kumiya, E. Walinda, H. Ueno, K. Ikeda, H. Sumiya, H. Tochio, Y. Yoshinari, Y. Harada and M. Shirakawa, *J. Am. Chem. Soc.*, 2020, **142**, 7542–7554.
14 J. Choi, H. Y. Zhou, R. Landig, H. Y. Wu, X. F. Yu, S. E. Von Stetina, G. Kucsko, S. Mango, D. J. Needleman, A. D. T. Samuel, P. C. Maurer, H. Park and M. D. Lukin, *Proc. Natl. Acad. Sci. U. S. A.*, 2020, **117**, 14636–14641.
15 M. Fujiwara, S. Sun, A. Dohms, Y. Nishimura, K. Suto, Y. Takezawa, K. Oshimi, L. Zhao, N. Sadzak, Y. Umehara, Y. Teki, N. Komatsu, O. Benson, Y. Shikano and E. Kage-Nakadai, *Sci. Adv.*, 2020, **6**, eaba9636.
16 D. A. Simpson, E. Morrisroe, J. M. McCoey, A. H. Lombard, D. C. Mendis, F. Treussart, L. T. Hall, S. Petrou and L. C. L. Hollenberg, *ACS Nano*, 2017, **11**, 12077–12086.
17 A. U. Khan, M. Khan, M. H. Cho and M. M. Khan, *Bioprocess Biosyst. Eng.*, 2020, **43**, 1339–1357.
18 K. Nagata, M. Nishimura, K. Daino, Y. Nishimura, Y. Hattori, R. Watanabe, D. Iizuka, A. Yokoya, K. Suzuki, S. Kakinuma and T. Imaoka, *J Radiat Res*, (in revision).
19 T. Yanagi, K. Kaminaga, W. Kada, O. Hanaizumi and R. Igarashi, *Nanomaterials*, 2020, **10**, 2282.
20 V. M. Acosta, E. Bauch, M. P. Ledbetter, A. Waxman, L.-S. Bouchard and D. Budker, *Phys. Rev. Lett.*, 2010, **104**, 070801.
21 R. Igarashi, Y. Yoshinari, H. Yokota, T. Sugi, F. Sugihara, K. Ikeda, H. Sumiya, S. Tsuji, I. Mori, H. Tochio, Y. Harada and M. Shirakawa, *Nano Lett.*, 2012, **12**, 5726–5732.
22 T. Yanagi, K. Kaminaga, M. Suzuki, H. Abe, H. Yamamoto, T. Ohshima, A. Kuwahata, M. Sekino, T. Imaoka, S. Kakinuma, T. Sugi, W. Kada, O. Hanaizumi and R. Igarashi, *ACS Nano*, 2021, **15**, 12869–12879.
23 S. Krause, A. Brock and D. E. Ingber, *J. Vis. Exp.*, 2013, (80), e50692.
24 D. Terada, T. Genjo, T. F. Segawa, R. Igarashi and M. Shirakawa, *Biochim. Biophys. Acta, Gen. Subj.*, 2020, **1864**, 129354.
25 H. S. Jung and K. C. Neuman, *Nanomaterials*, 2021, **11**, 153.
26 H. Ali, S. Ali, M. Mazhar, A. Ali, A. Jahan and A. Ali, *Photodiagn. Photodyn. Ther.*, 2017, **19**, 37–44.
27 Y. Kirihara, M. Takechi, K. Kurosaki, Y. Kobayashi, Y. Saito and T. Takeuchi, *Exp. Anim.*, 2016, **65**, 27–36.
28 E. M. Palsson-McDermott and L. A. O'Neill, *Immunology*, 2004, **113**, 153–162.
29 V. Tseeb, M. Suzuki, K. Oyama, K. Iwai and S. Ishiwata, *HFSP J.*, 2009, **3**, 117–123.
30 N. Wang, G.-Q. Liu, W.-H. Leong, H. Zeng, X. Feng, S.-H. Li, F. Dolde, H. Fedder, J. Wrachtrup, X.-D. Cui, S. Yang, Q. Li and R.-B. Liu, *Phys. Rev. X*, 2018, **8**, 011042.
31 M. B. Rakhunde, S. Gotarkar and S. G. Choudhari, *Cureus*, 2022, **14**, e31251.
32 M. Sathiyabarathi, S. Jeyakumar, A. Manimaran, G. Jayaprakash, H. A. Pushpadass, M. Sivaram, K. P. Ramesha, D. N. Das, M. A. Kataktalware, M. A. Prakash and R. D. Kumar, *Vet. World*, 2016, **9**, 1075–1081.
33 K. Okabe, R. Sakaguchi, B. Shi and S. Kiyonaka, *Pflugers Arch.*, 2018, **470**, 717–731.
34 T. Sekiguchi, S. Sotoma and Y. Harada, *Biophys. Physicobiol.*, 2018, **15**, 229–234.
35 Y. Nakamura, J. Kubota, Y. Nishimura, K. Nagata, M. Nishimura, K. Daino, A. Ishikawa, T. Kaneko, T. Mashimo, T. Kokubo, M. Takabatake, K. Inoue, M. Fukushi, M. Arai, M. Saito, Y. Shimada, S. Kakinuma and T. Imaoka, *Cancer Sci.*, 2022, **113**, 3362–3375.
36 T. Imaoka, M. Nishimura, K. Doi, S. Tani, K. Ishikawa, S. Yamashita, T. Ushijima, T. Imai and Y. Shimada, *Int. J. Cancer*, 2014, **134**, 1529–1538.
37 T. Imaoka, M. Nishimura, K. Daino and S. Kakinuma, *J. Radiat. Res.*, 2023, **64**, 273–283.